Dual-high-frequency from single-piezoelectric crystal for ACE degradation by hybrid advanced oxidation UV-sonochemistry process

Fabiola Mendez-Arriaga [a,b,*], Chad D. Vecitis [b]

[a] CONACyT Consejo Nacional de Ciencia y Tecnología & ICAT-UNAM, CdMx, 04510, Mexico
[b] John A. Paulson School of Engineering and Applied Sciences, Harvard University, Cambridge, MA 02138, US

ARTICLE INFO

ABSTRACT

This study investigates the combination of two waves emitted from a single-piezoelectric crystal by use of a dual-frequency generator in a sonochemical reactor. The dual-frequency configurations analyzed were the double-modulated fundamental frequency (376–376 kHz), resonant and second harmonic, termed 376D, 376R and 376H respectively. The effect of the phase shift (Φ) and the percentage of modulation between added waves were described by the total acoustic power distribution (P_t) measured inside the sonoreactor. Moreover, optimal angle alignment and modulation between dual-frequency waves for 376D, 376R and 376H cases were selected in order to evaluate the ultrasonic synergy by sonochemical reactivity in production of H_2O_2, in degradation rate of a model emerging pollutant ACE, and in the TOC and biodegradability evolution in the treated effluent. Phase shift and percentage of modulation had strong effect on the resulted waveform and on the sonochemical efficiency for all, harmonic and non-harmonic, dual-frequency combinations created. In the 376D case, the best reinforcement conditions are founded at 0° and 360°. In the 376H the maximum power distribution presents a 90° period. Shift phase does not determines any cyclic pattern in the total power distribution for the 376R case. The highest H_2O_2 production rate was observed for the 376H case followed for 376D and 376R configurations with 1.61, 1.12 and 0.58 μM/min by angle alignment in 105, 0 and 110° respectively. The highest initial degradation rate of ACE was observed for the 376D case followed for 376H and 376R with 0.56, 0.42 and 0.33 μM/min at 100% modulation. Reduced mineralization was observed in all dual-frequency configurations (8.54% for 376D and approximately 4.5% for 376R and 3756H modes). Contrasting results are observed regard to biodegradability ratio following the next sequence 376D < 376H≈376R with 0.9, 2.30 and 2.33 respectively. Relevant intensification in hydroxyl radicals production is observed by the UV-US system increasing up three folds the ACE removal and mineralization and two folds higher biodegradability of effluent in particular for 376R and 376H cases at optimal operation condition of dual-frequency signal.

1. Introduction

Some of the most common artificial sweeteners such as acesulfame (ACE), aspartame, saccharin, and sucralose have been found as contaminants in the environment [1]. They are continuously introduced into natural aquatic systems via wastewater treatment plant influents and/or effluents due to humans cannot metabolize them neither by microorganisms in activated sludge. In particular, ACE has proven to be one of the most persistent sugar substitutes commonly detected in surface waters in countries such as Switzerland, Germany, Austria, Canada, USA, China, Finland, and Israel among others [1–4]. Accumulation of sweeteners in the environment could result in harmful ecosystem impact since they mimic artificially natural chemicals during the photosynthesis in zooplankton and vascular plants [5].

Effectiveness of different conventional water treatments (flocculation, biodegradation, ozonation, activated carbon filtration, reverse osmosis, chlorination/chloramination, etc.) has shown limitations on removal and degradation of sweeteners [6–9]. For instance, under typical waterworks conditions, ozone removes ACE incompletely only between 18 and 60% [8]. On the other hand, due to the high solubility of ACE in water, several adsorption treatments are very limited and strongly depended on the adsorbent preload. For example, ACE was

detected up to 0.76 μg/L by use of 30 m^3/kg of granulated activated carbon filters [8,10].

On the other hand, scarce number of advanced oxidation processes (AOPs) have been examined as alternative processes for removal of this specific sort of emerging contaminants [12]. AOPs are mainly based on the presence and reactivity of the hydroxyl radical (•OH) generated at standard ambient temperature and pressure (25 °C and 1 atm) with or without catalyst and/or presence of chemically reactive energy with or without extra oxidants reagents, such ferrate or persulfate [11]. Among the AOP's, the heterogeneous photocatalysis with TiO$_2$ [13], Fenton and photoFenton reaction, UV-H$_2$O$_2$, alkaline O$_3$ process and ultrasound irradiation (US) have shown highlighted efficiencies on removal of a wide type of persistent, recalcitrant, and emergent contaminants [11,12,14]. US is generated via acoustic cavitation i.e., the rapid (<ms) formation, growth, and quasi-adiabatic collapse of microbubbles due to interaction with the ultrasonic waves above 20 kHz [15]. The exposition of ultrasonic waves through a liquid medium promotes alternating compression and rarefaction cycles. During the rarefaction cycle, a void is formed containing the liquid vapor, dissolved gases and volatile solutes. During the compression cycle, the cavity is compressed resulting in high temperatures and pressures within the bubble. During the transient bubble collapse the PdV energy of bubble expansion is converted to internal energy of the bubble vapor resulting in average gas phase temperatures of ~3800 °C and surface temperatures of ~527 °C [23]. The extreme bubble vapor T results in pyrolysis of the molecules present inside the bubble and in production of strong oxidants such as the •OH from thermolytic water dissociation:

$$H_2O +))) \rightarrow \bullet H + \bullet OH \qquad (1)$$

In presence of oxygen, the perhydroxyl radical is also promoted:

$$\bullet H + O_2 \rightarrow \bullet OOH \qquad (2)$$

The radicals formed are diffused in the solution and simultaneously H$_2$O$_2$ is formed from the combination of •OH and •OOH:

$$2\bullet OH \rightarrow H_2O_2 \qquad (3)$$

$$2\bullet OOH \leftrightarrow H_2O_2 + O_2 \qquad (4)$$

The chemical reactions during a cavitational event take place in the gas phase at the center of the collapsing cavity, in the bulk of the liquid solution and/or in the interfacial region. The preferential reaction zone depend strongly on the operating parameters, the reactor geometry and the hydrophilic or hydrophobic character of the initial organics and byproducts generated along the US treatment [16,17].

The H$_2$O$_2$ reagent, as byproduct of the •OH sonorecombination, could represent an extra source of •OH if UV irradiation (254 nm) is engaged after or during the US treatment:

$$H_2O_2 + UV_{254} \rightarrow 2\bullet OH \qquad (5)$$

Thus the UV-US hybrid process is a promising promoter of highly reactive •OH able to react unselectively against emergent persistent pollutants. The vast majority of applications of US for degradation of contaminants have been developed by use of a unique source of irradiation with one piezo emitter or with multi-crystals placed in different inter faces inside the sonoreactor. In both cases, the emission of the single frequency at specified intensity is the most common configuration founded in literature [11,18–20]. However, the sonochemical activity by generation of dual-high-frequency signal as product of addition or combination of two pure waves emitted from a single piezoelectric crystal has been considerably less analyzed at laboratory scale [14]. In additive configuration, two or more single individual waveforms are combined in order to produce a new controlled signal. Cavitation bubbles created from the emission of a dual-frequency signal have different

dynamic properties than the bubbles formed under single frequency emission [30]. Main characteristics of the new resulting waveform depend on the original frequencies, amplitudes, percentage of modulation and phase angle between signals. Previous works have observed enhancement of sonochemical activity by application of dual-frequency radiation such as Kawabata and Umemura (1996 and 2003), Linzheng et al., (2021), Kálmán (2021), Kanthale et al., (2008), Waldo et al., (2018) and Baraldi et al., (2007). In particular, the analysis of the second harmonic superimposed signal (SHS) has given theoretical and experimental support to assure that the lower frequency promotes higher nuclei formation events while the high frequency leads to bubble collapse [14,21,26–31]. For example, Kawabata and Umemura (1996 and 2003) [21,27] suggest that each frequency signal in the SHS case is effective for different stage of cavitation including the growth, dissipation and collapse of microbubbles [21]. They assure that SHS signal results more effective for the growth of the bubble and the fundamental signal enhances the cavitation collapse since the resonant bubble size increases as the ultrasound frequency decreases [27]. In addition, Waldo and Vecitis (2018) [26] assure that the SHS signal yields a waveform that maximizes bubble radial motion enhancing rectified diffusion and the rate and intensity of cavitation events under optimal power distribution and phase shift conditions. Moreover, they demonstrated experimentally that the increased efficiency of sonochemical reactivity was possible by control of the dual-high-frequency signal in a batch ultrasound reactor producing up to a threefold increase in H$_2$O$_2$ generation [14]. They concluded that dual-frequency synergy depends on the specific interactions between the frequencies, power distributions, and phase shifts [14]. Theoretical and experimental elucidation of the sonodynamics enhancement by use of single-source dual-frequency signal are still prominent areas of research for the ultrasonochemistry sciences.
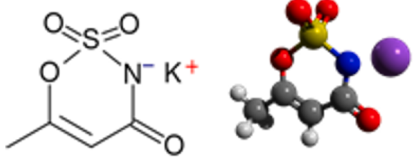
Therefore, the objective of this work is to evaluate the cavitation efficiency of a dual-high frequency signal emitted from a single piezoelectric crystal by analysis of the resulted power distribution inside the sonoreactor by varying the phase angle (Φ) and percent of modulation between two signals. Three specific cases of study were considered: 1) double-added fundamental frequency (376–376 kHz), 2) resonant-added frequency (376–728 kHz), and 3) second harmonic-added frequency (376–752 kHz), termed as 376D, 376R and 376H respectively. Moreover, optimal phase angle and modulation between dual-frequency wave for D, R and H cases were selected in order to evaluate the sonochemical reactivity in production of H$_2$O$_2$, in degradation of a model emerging pollutant ACE, and in the TOC and biodegradability evolution for the treated effluent. Effect of gas sparring and spatial distribution of hydroxyl radical by luminol test were also included for the sonoreactor characterization. Finally, the residual H$_2$O$_2$ was considered an extra source of hydroxyl radicals by exposition of UV irradiation in order to evaluate the UV-US hybrid advanced oxidation process under optimal conditions previously founded for D, R and H cases.

2. Experimental methods

2.1. Materials

ACE-K (potassium 6-methyl-1,2,3-oxathiazine-4(3H)-one 2,2-dioxide) was purchased from Fluka and used as received (see Table 1). Sodium hydroxide and sulfuric acid concentrated solutions (Sigma-Aldrich) were used to adjust at desired pH. Argon, air and oxygen (Ultrahigh purity, Airgas) were used without previous treatment. Potassium iodide and ammonium molybdate salt (both Sigma-Aldrich) were employed for H$_2$O$_2$ quantification and luminol (Sigma) reagent was employed for visual hydroxyl radical image. Deionized water (DW, 18.2 MΩ/cm resistivity) was obtained using the Milli-Q gradient water purification system (Millipore).

Table 1

Physicochemical properties of ACE.

Acesulfame K (ACE) potassium 6-methyl-2,2-dioxo-2H-1,2λ6,3-oxathiazin-4-olate	
	https://commons.wikimedia.org/wiki/File:Acesulfame-k-ball-and-stick.png https://commons.wikimedia.org/wiki/File:Acesulfame-k-ball-and-stick.png
CAS no.	55589-62-3
Molecular formula	$C_4H_4KNO_4S$
Appearance	White crystalline powder
Density (g/cm^3) at 25 °C and 100 kPa	1.81
Melting point (°C)	225
Molecular weight (g/mol)	201.24
Water solubility (g/L) at 20 °C	270
ADI as K salt (mg/kg body weight)	9
Sugar equivalence	200
pK_a	2.0
Log K_{OW}	−1.33
Human excretion	100% unchanged

2.2. Reactor

Ultrasonic experiments were performed in a 1.3 L batch reactor composed of a jacketed glass vessel (Chemglass) and a round piezo-electric crystal (5 cm diameter, 0.35 cm thick, PZT-840; APC International) attached to a steel plate (12.7 cm diameter, 0.05 cm thick) on the right side of the glass reactor (see Fig. 1) using a conducting silver epoxy. The electrical lead was connected to the piezo using a non-lead solder. The solution in the reactor was magnetically stirred and sparged with gas for 20 min prior to and during the reaction. The temperature was controlled with a recirculating chiller (ThermoScientific). Single or added signals were driven by an arbitrary waveform generator (33522A Agilent, 2-Ch, 250 MSa/s). The resulting waveform was sent to the oscilloscope (Aglient, 54621A, 200 MSa/s) and to the linear RF power amplifier (2100L, 120 W electrical output max, 10 KHz-12 MHz, E&I Ltd.). UV-ultrasound hybrid process was developed by simultaneous UV irradiation by immersion of a Hg lamp with centered emission in the UV-C band at 253.7 and 185 nm, 90–10% respectively (97–0067-01-UVP, 115 V-60 kHz, 4.5 mW/cm^2).

2.3. Analyses

ACE concentration and H_2O_2 evolution were determined by spectrophotometric analysis (Scinco, S3100) at 226 and 350 nm, respectively. TC, TOC and IC measurements were completed on a Shimadzu TOC-VWS instrument. pH was recorded by a pH meter WTW 7110. Hg- thermometer was employed for calorimetric determinations. BOD_5 (OxiTop instrument) determinations were carried out according to the standard methods. Data logger instrument (LabPro Vernier) was used to measure the online input/output of voltage and current. All experiments were carried out at least twice.
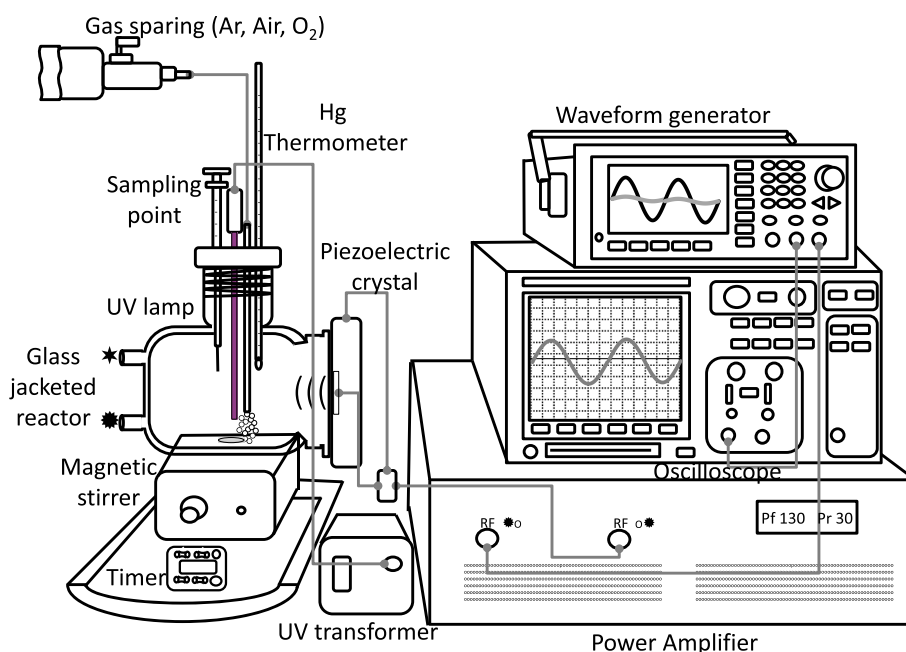

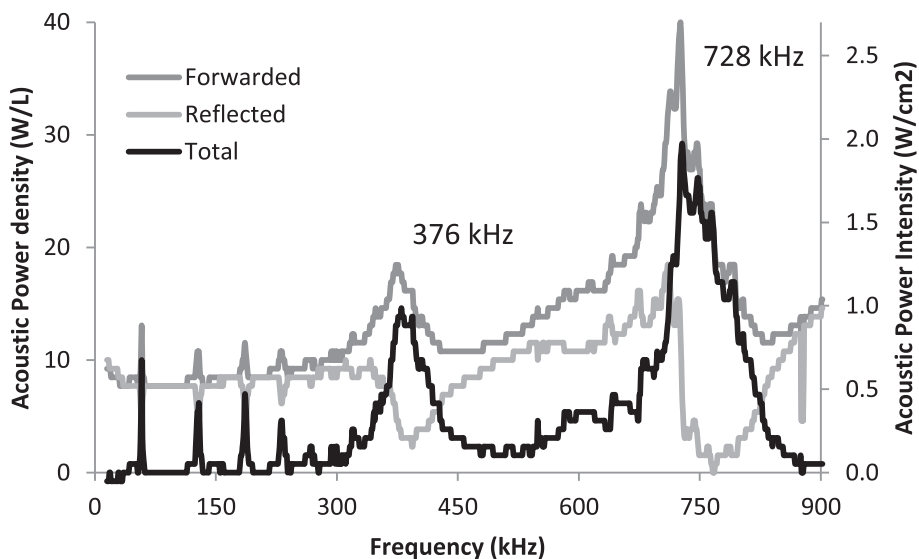
Fig. 1. Reactor and instruments.

Fig. 2. Acoustic Power Density and Intensity answers for the applied frequency inside the range of 15 to 900 kHz. Sine waveform, 1.3 L DW total volume, without gas sparing, 1 V_{pp} = 0.347 V_{rms}. Acoustic power forwarded (P_f ▬), acoustic power reflected (P_r ▬) and total acoustic power (P_t ■).

Table 2
Parameters of the original waves and the resulted waveforms for D, R and H cases at 0o phase angle aligned and 100% sum type modulation.

	Frequency kHz	Amplitude V_{pp} (V_{rms})	Resulting waveform (wave 1 + wave 2) fundamental + added
Double 376D	Fundamental signal Wave 1 376	Fundamental signal Wave 1 2.8 (0.98)*	
	Added signal Wave 2 376	Added signal Wave 2 2.5 (0. 088)	
Resonant 376R	Fundamental signal Wave 1 376	Fundamental signal Wave 1 3.5 (1.23)	
	Added signal Wave 2 728	Added signal Wave 2 3.0 (1.05)	
Second Harmonic Superimposed 376H	Fundamental signal Wave 1 376	Fundamental signal Wave 1 4.0 (1.41)	
	Added signal Wave 2 752	Added signal Wave 2 3.0 (1.05)	

·········Fundamental signal, ----Added signal, ▬▬ Double modulated signal resulted.

······Fundamental signal, ——Added signal, ■■ Double modulated signal resulted.

3. Results

3.1. Previous resonant frequency determination

As possible to observe in Fig. 1, the piezoelectric disk is attached to a stainless steel plate transducer and clamped to the glass sonoreactor. The resonant frequency of the piezoelectric disk specified by the manufacturer was 600 kHz. At resonant frequencies, the system stores vibrational energy, even small periodic driving forces producing large amplitude oscillations. Some systems have multiple dissimilar resonant frequencies. In order to establish the particular characteristic resonant frequency of the piezo transducer system here employed, a constant supply of 0.340 $V_{root\ mean\ square}$ (V_{rms}) equal to 1 $V_{peak\ to\ peak}$ (V_{pp}) of a sine wave was programmed in the waveform generator and the

frequency was scanned manually from 15 to 900 kHz. The output of the arbitrary waveform generator was sent to the RF amplifier and subsequently sent to the piezoelectric crystal mounted to the sonoreactor. Fig. 2 shows the acoustic power density and intensity forwarded (P_f), reflected (P_r) and total (P_t), recorded from the RF amplifier, as function of the frequency applied and released to 1.3 L of deionized water as total volume in the sonoreactor. Total acoustic power (P_t) was assumed as the difference between the forwarded (P_f) and reflected (P_r) power.

As possible to observe, the first resonant peak was founded at 376 kHz. The piezoelectric materials usually have more than one resonance frequency, especially at integer multiple of the fundamental frequency (harmonics) of the strongest resonance, arithmetically expected at 752 kHz. However, the second acoustic resonant power was observed earlier at 728 kHz. The piezoelectric crystal here employed does not replicate
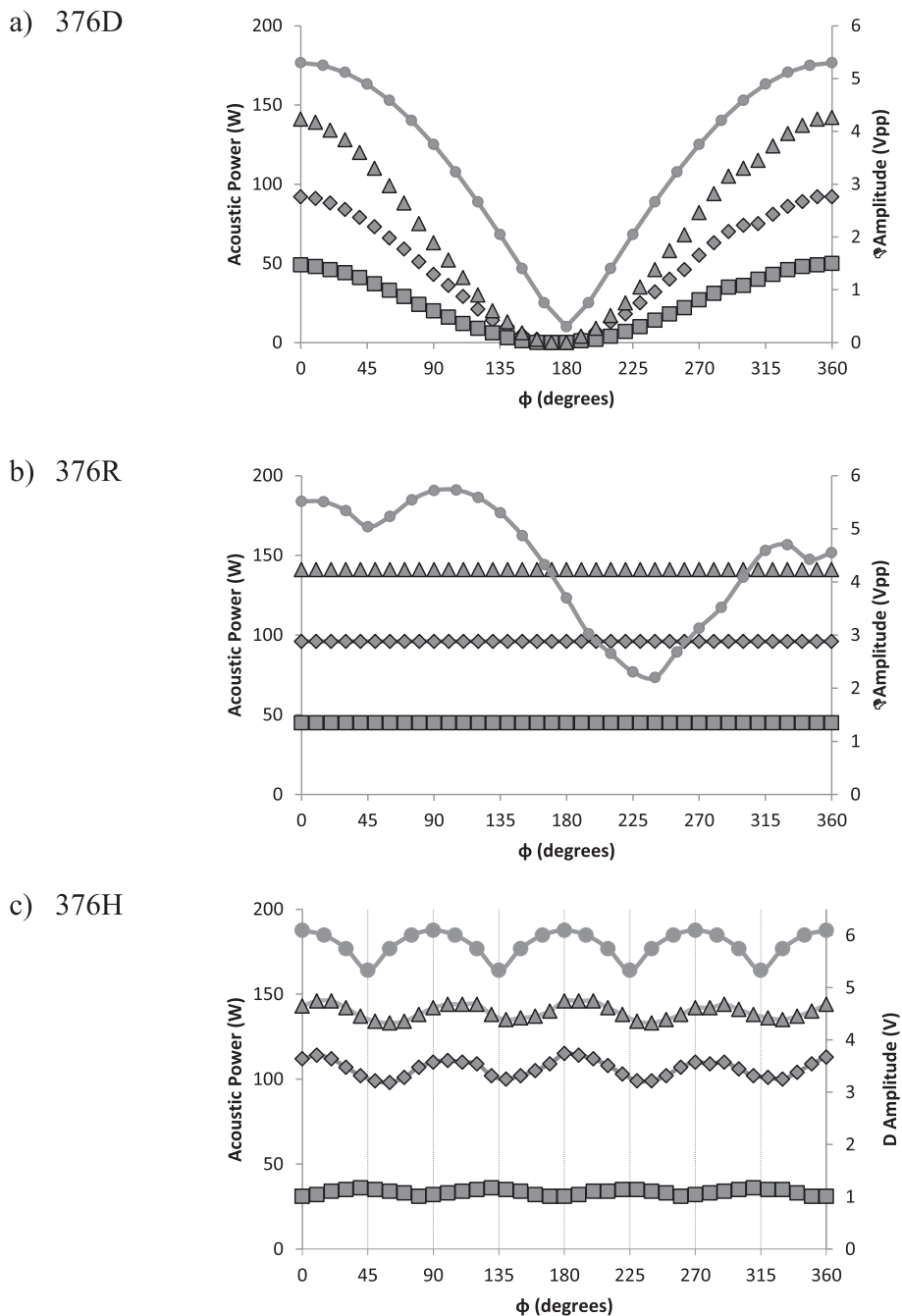

Fig. 3. Angle phase (Φ) effect (ranging from 0° to 360°, 10° step) on acoustic power distribution (P_t (♦), P_f (▲) and P_r (■)) with the corresponding ΔAmp (●) resulted for D (a), R (b) and H (c) modulated cases. 100% sum type modulation. Ar as saturated gas, 1.3 L total volume DW and 6 °C controlled temperature.

the highest acoustic power at its second harmonic as expected into the range of frequency tested probably due to the imperfections and impurities of the original material.

Thus, frequencies of the signals studied were settled as the fundamental, resonant and second harmonic for 376, 728 and 752 kHz respectively. The nomenclature here used to name the double-frequency signal generated was determined as 376D, 376R and 376H to describe the double, the resonant and the harmonic signals respectively all of them added to the fundamental frequency (376 kHz).

The amplifier yields max around 120 W linear output power. P_t was adjusted below to this max limit for each added D, R or H case. Parameters and main characteristics of both, the original and resulted double-modulated waveforms, are detailed in Table 2. The last column in Table 2 shows the resulting waveform from the added signals and the amplitudes reached at initial alignment to 0° as phase shift (i.e., both original waves starting at the 0° position) and 100% of modulation (i.e. total fraction of second signal added to the fundamental wave). Addition of the dashed lines results in the unbroken line, which clearly has a more complex pattern than both pure signals. The complex new pattern repeats with the same period of the highest common integer factor for cases 376D and 376H.

3.2. Angle phase (Φ) effect on acoustic power distribution

In order to evaluate the effect of the lag point between signals (degrees alignment between fundamental and added signal) on the power dissipation into the sonoreactor (P_t, P_f and P_r), the angle shift was scanned from 0 to 360° every 10° maintaining 100% constant modulation between both signals. Total volume of DW in the sonoreactor was 1.3 L and the initial temperature was adjusted at 6 °C. The amplifier operates in the range of 0 to 180° with the following ratios: $V_{Output} \approx 12.59 \, V_{Input}$, $I_{Output} \approx 0.0035 \, I_{Input}$. In Fig. 3 is depicted the P_t, P_f and P_r distribution dissipated to the liquid for the 376D, 376R and 376H cases between $0° < \Phi < 360°$. The acoustic power distribution depends on the characteristic frequency and amplitude (peak-to-peak voltage) resulted from the double signal especially for 376D and 376H configurations as possible to observe in Fig. 3. The case 376D (same frequency and initially close similar amplitude) produces total reinforcement in 0° and 360° (completely "in phase") with a resulting amplitude almost twice than the settled initially. On the other hand, the 180° angle phase alignment (completely "out of phase") results in nearly complete cancellation between both. Total cancelation would be observed if both signals were settled exactly at the same initial amplitudes. As expected, symmetric responses of acoustic power are observed from 0 to 180° concomitantly to the range 180 to 360°. Similar symmetric response is observed for the acoustic power in the case 376H with a period of 90° following the parallel resulting amplitude pattern along the complete cycle. The harmonic case reinforces and cancels partially the effect of the acoustic power in a lesser extent than in the case 376D. In the case 376R, the Φ alignment does not have effect on the P_t, P_f and P_r answer remaining constant in 97, 144 and 47 W respectively along the whole cycle. Over large number of cycles, only the D and H cases replicate the power distribution and ΔAmp. The variation of the angle alignment results in remarkable differences between the max and min peak-to-peak voltage (●) of the resulting waveform Δ (ΔAmp): 5.0, 3.54 and 0.76 for 376D, 376R and 376H cases respectively. Moreover, 376H configuration registers the lowest P_r distribution compared with the analogous acoustic powers for 376D and 376R cases: $P_{r\,max}$ for both 376D and 376R resulted was 50 W and 37 W for the 376H case.
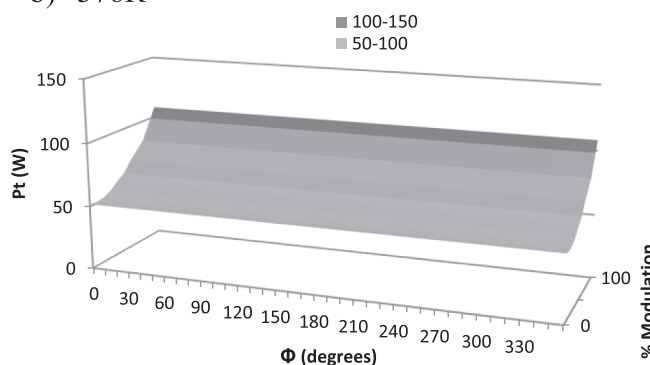
3.3. % modulation effect on acoustic power distribution

In order to evaluate the effect of the portion of addition of the second signal to the fundamental, percentage of modulation was scanned from 0 to 100% varying simultaneously the angle phase between both signals from 0 to 360° every 10° step. Fig. 4 shows the percentage of modulation
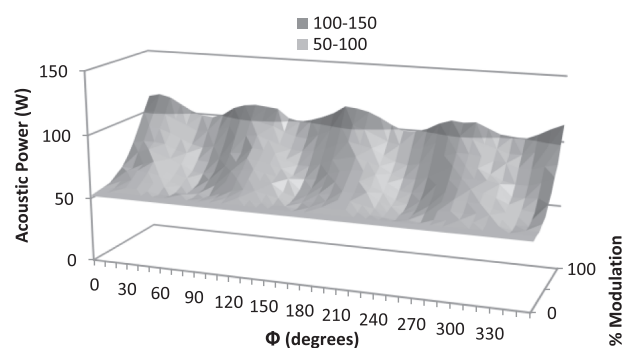
a) 376D
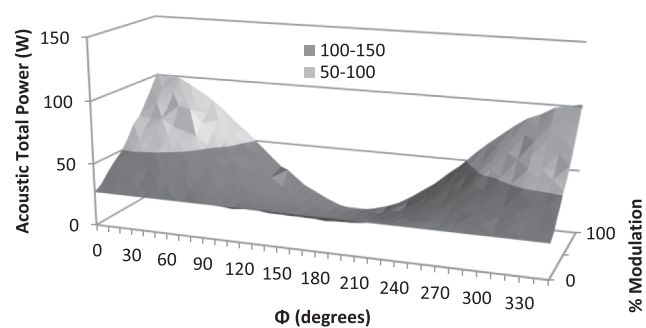
b) 376R

c) 376H

Fig. 4. % of modulation effect (from 0 to 100%) on total power distribution P_t for a) 376D, b) 376R and c) 376H cases scanned from 0° to 360° angle shift, 10° step. Ar as saturated gas, 1.3 L total volume DW and 6 °C controlled temperature.

effect on P_t for 376D, 376R and 376H cases. As expected, it is possible to observe that P_t increases directly proportional as increase the percentage of modulation in all cases. Moreover, analogues patterns of Φ variation are observed along the modulation scan. At modulation lower than 20% the acoustic power distribution (forwarded and reflected) register the lowest levels of power dispersion remaining unchanged in all cases because it is equivalent to release the fundamental signal. As expected, the 100% addition of the second signal results in the highest values of acoustic power dispersed inside the sonoreactor.

3.4. Saturation gas effect on acoustic power distribution

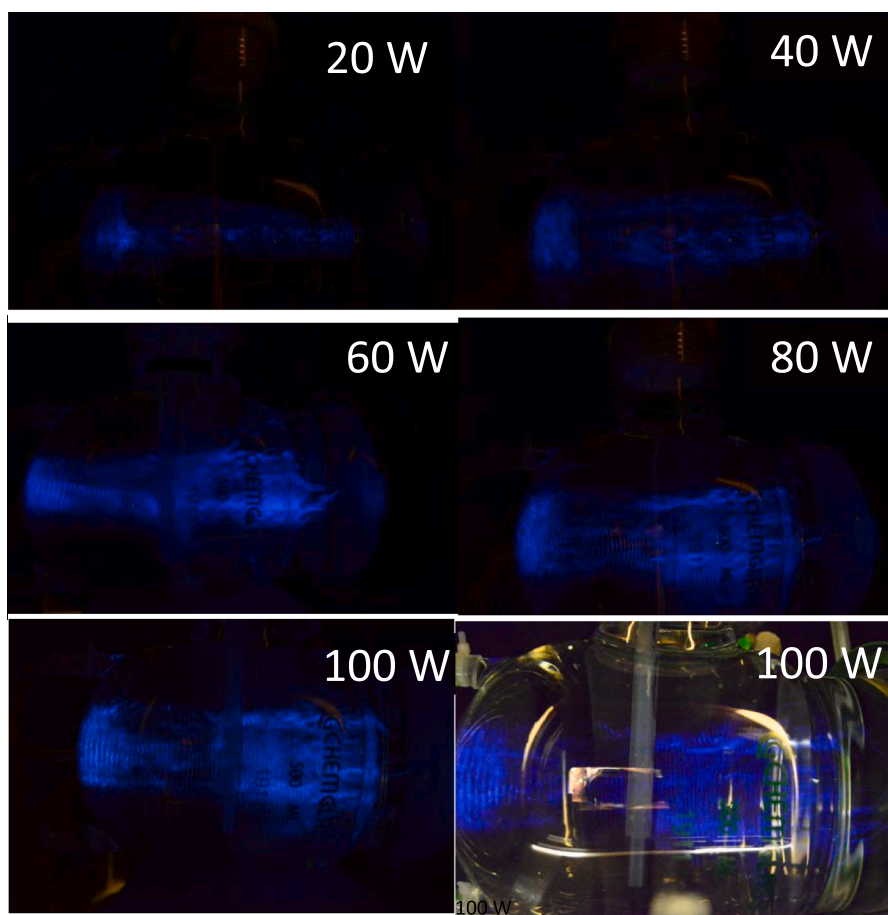Experiments to evaluate the effect of saturating gases on P_t, P_f and P_r

Fig. 5. Captions of hydroxyl radical spatial distribution inside the sonoreactor at 20, 40, 60 80 and 100 W of total power dissipation (equivalent to 2.75, 3.80, 4.60, 5.25 and 5.8 Vpp respectively) for 1.3 L DW high frequency irradiated at 376 kHz, Ar sparring gas, controlled 6 °C and constant magnetic stirring.

dispersion were carried out varying % modulation and Φ alignment for D, R and H cases. Ar, air and O_2 pure gases were sparred until saturation in 1.3 L of DW at least 10 min before and during dual-frequency emission. The acoustic power distribution does not change by presence of different types of gas saturation along the phase shift and fraction of modulation ranges tested (data not shown). In addition, at free O_2 consumption without continue sparring of any gas, the P_t, P_f and P_r dispersion is unaltered. However, as expected the H_2O_2 generation rate was higher in presence of Ar as saturating gas than the observed under O_2 (Supplementary material S1).

3.5. Visual spatial volumetric reactivity by hydroxyl radical distribution

Visual presence of •OH was photographed by luminol luminiscence effect in order to evaluate the uniformity of the energy dissipation inside the sonoreactor [22]. Those experiments were carried out with fresh luminol solution (0.001 M) in 1.3 L of DW magnetically stirred, pH 11, Ar gas saturated atmosphere and 6 °C. Photos were obtained inside a homemade full darkbox in order to improve the visual illustration. In Fig. 5 is possible to observe photographs taken instantaneously after application of a sine wave of 376 kHz varying the acoustic power dissipation from 20 to 100 W, 20 W step, equivalent to the range between 2.75 and 5.8 Vpp respectively. The wave applied is dispersed horizontally into the reactor in dread forms with highlighted compression/rarefaction zones visually observed on the partial sphere-shaped left wall of the sonoreactor. As possible to observe the enhancement on emission intensity is power dependent. With the lower power applied the ultrasonic irradiation (20 W) comes from the central section of the transducer, however in the case of the 100 W the visual blue emission is

radial extended from the transducer plate. Since the wavelength is much smaller than piezo diameter, the acoustic plane wave initially shrinks in diameter before expanding again causing there to be a higher acoustic power density some distance from the piezo surface. It can be noted that the space homogeneous distribution of •OH is not full reached in the volume of the reactor and sections in reactor there will be shortage of hydroxyl radical. However, both the constant magnetic stirring of the 1.3 L DW and the continuous sparring gas promote efficient mass transfer of reactants to the bulk of the solution.

3.6. Sonochemical energy efficiency (η)

In order to determine the fraction of which is actually utilized for the generation of cavities as well as those dissipated in heat form, calorimetric tests were carried out into 1.3 L DW without temperature control neither gas sparring at fundamental irradiation 368 kHz for 50 W of power supplied to the system. The acoustic power transferred to the medium and transformed to heat was estimated in 39.54 W. Thus, the sonochemical efficiency η was estimated in 24% [18,22]. Such result agrees the reported efficiencies according to Pandit and Gogate (2006) for ultrasonic devices through multiple transducers with double or triple frequency cells, with characteristic sonochemical energy efficiencies between 25 and 44% depending of the specific configurations [19,20].

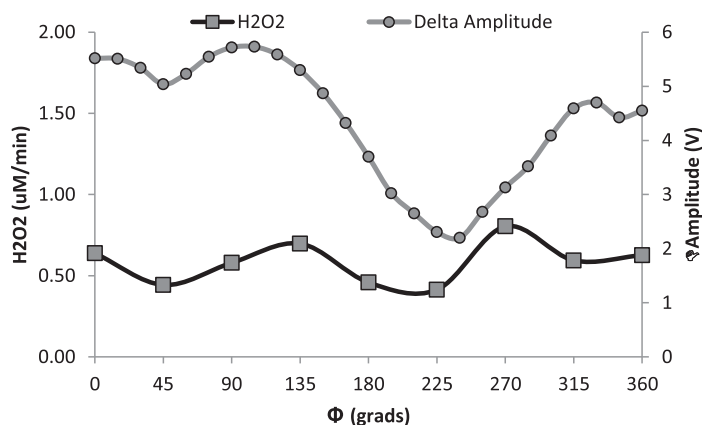### 3.7. Angle phase alignment (Φ) effect on H_2O_2 production

Fig. 6 shows the production rate of H_2O_2 varying the angle phase for 376D, 376R and 376H cases, 100% modulated signal. As possible to observe, the H_2O_2 generation depends on the Φ alignment and the total
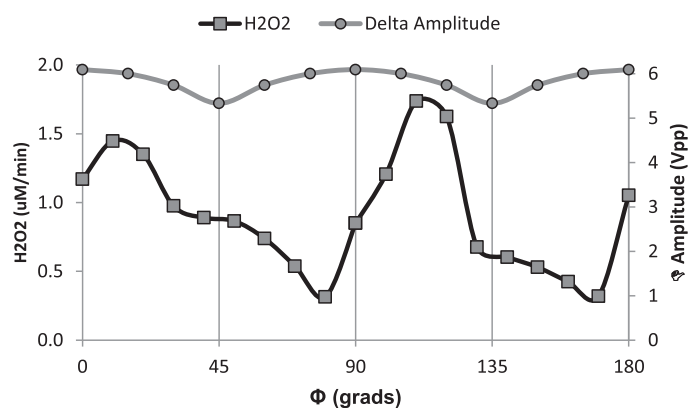
a) 376D
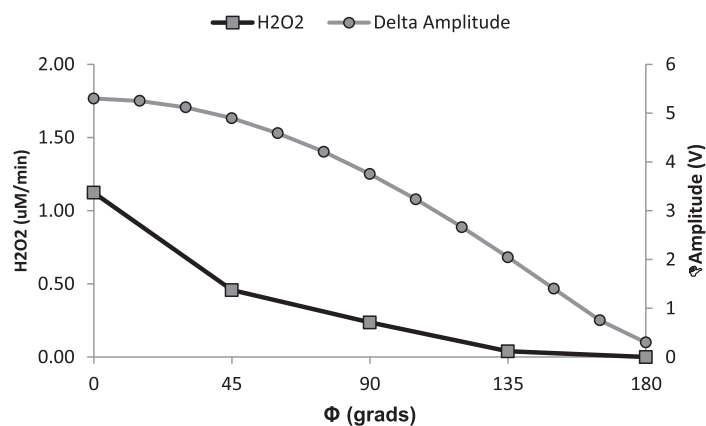
b) 376R

c) 376H

Fig. 6. Angle phase (Φ) effect on H_2O_2 production. a) 376D, b) 376R and c) 376H at 100% modulation, saturated gas Ar, 1.3 L total volume DW and initial 6 °C temperature controlled.
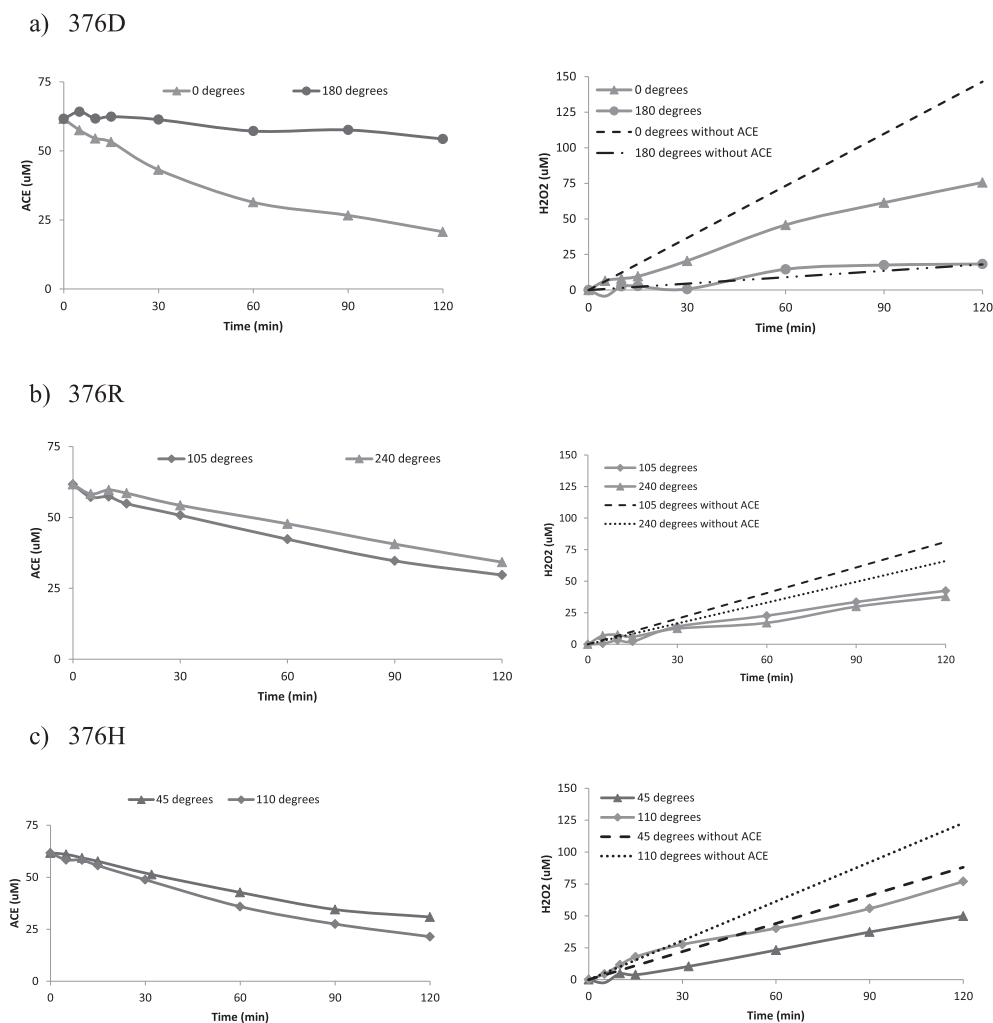
acoustic power dissipation reached. Clearly, in the case 376D the H_2O_2 production rate is direct proportional to total acoustic power applied. As higher peak-to-peak voltage amplitude resulted from addition of signals, higher H_2O_2 production rate is observed. Maximum and minimum H_2O_2 production rates are reached for 1.12 and 0.3 μM/min respectively. It is important to note that the change in the angle phase does not change the resulting wave shape nonetheless it changes the amplitude and the concomitant power released to the liquid. The resonant case shows an erratic behavior close correspondent to the acoustic power applied however, the intensity does not reflect the differences between H_2O_2 production rate. For example, around 210 and 255° it could be expected

the lowest ratio of production regarding to the lowest values of acoustic power applied and between 75 and 120° it could be expected the highest H_2O_2 production rate. Nevertheless, the resulted average of H_2O_2 rate is 0.58 μM/min with a standard deviation of 0.12 μM/min. It is possible to assure that the constant power behavior determines strongly the H_2O_2 generation and only in lesser extension the resulting waveform affect the compression and rarefaction steps of the cavitation phenomena. It is important to note that the case 376R does not replicate periodically analogous waveform at any angle shift. In the case of 376H shorten intervals of phase sifth Φ -every 10°- were necessary to test and zooming its effect on H_2O_2 production. The harmonic case shows a direct

Table 3
Sonochemical reactivity for 376D, 376R and 376H configurations.

	Φ (°)	Initial degradation rate k_{ACE} (vM/min)	ΔH_2O_2 (μM)	•OH reactivity (μM)	ACE/ACE$_o$ 120 min	OH/ACE μM/μM	TOC removal 120 min (%)	BOD$_5$/BOD$_{5,}$ ACE10mg/L 120 min
376D	0	0.5673	70.8	141.6	0.67	3.45	8.54	0.9
	180	0.0706	0.90	1.8	0.12	0.24		
376R	105	0.3330	38.8	77.6	0.52	2.43	4.74	2.33
	240	0.1583	28.2	56.4	0.45	2.05		
376H	110	0.4273	45.86	92.0	0.65	2.33	4.37	2.30
	45	0.3269	38.32	76.0	0.49	2.52		

a) 376D

b) 376R

c) 376H

Fig. 7. Phase shift (Φ) effect on ACE degradation and H$_2$O$_2$ evolution in presence and absence of substrate for a) 376D, b) 376R and c) 376H cases at 100% modulation, saturated gas Ar, 1.3 L total volume DW and initial 6 °C temperature controlled.

relationship between the waveform and the H$_2$O$_2$ generation rates every single 90° but without direct correspondence to the ΔAmp (0.76 between the max and min observed). From 0 to 45° (or 90 to 135°) ranges the angle of highest H$_2$O$_2$ production (1.40 ± 0.21 μM/min) following by a semi constant period around 45° (or 135°) with a decrease in the H$_2$O$_2$ rate in 0.80 ± 0.13 μM/min. The minimum rate, 0.3161 ± 0.003 μM/min, is observed for around 80 and 170° angle shift. In this case, the angle phase has the stronger effect on the resulted waveform. Thus, improvement of the cavitation efficiency is related to the compression and rarefaction events instead the acoustic power or amplitude resulted. The dual-frequency shape is replicated for 0 and 180°. In contrast, for 45 and 135° the waveform is replicated in the inverse form. The 90° has not duplicate waveforms into the 0-180° range.

3.8. Angle phase alignment (Φ) effect on ACE degradation

As possible to observe, the chemical reactivity in the ultrasonic process changes depending on several factors. In this case, for the modulated system the most important effects are the resulted wave shape depending on the angle phase between signals, the resulted amplitude and the acoustic power released to the medium. In order to study all integrated effects on ACE degradation, selection of different angle phases were chosen for 376D, 376R and 376H cases. For case 376D were selected the extreme points of acoustic power, it is at 0 and 180°. In the case 376R, even the acoustic power was constant, 105 and 240° were selected as the max and min amplitude values registered. In 376H case was selected the angle shirt in 45 and 110° in order to observe

different reactivity by H_2O_2 generation even consider that the acoustic power and amplitude do not shown a significant quantitative change. In Table 3 is possible to observe the characteristics of the applied waveform varying the angle phase as well as kinetic results for ACE degradation and H_2O_2 production. Fig. 7 shows the pseudo zero order degradation kinetic of ACE at different angle phase and the H_2O_2 evolution during reaction for 376D, 376R and 376H cases. As possible to observe the 376D case, with same sine wave shape, the reactivity is directly related to the acoustic power and amplitude applied. As expected, as higher amplitude resulted by the reinforcement at 0° higher initial degradation rate of ACE is observed. Under such conditions 67% of the pollutant is removed after 120 min of ultrasonic irradiation. In addition, difference between the H_2O_2 concentration in presence and absence of the organic is 70 µM (3.45 µM of •OH per µM of ACE). Decrease in acoustic power, as consequence of cancelation waveform at 180° results in lower degradation of the compound (12%) with a poor •OH consumption of 1.8 µM. On the other hand, in the 376R case the initial ACE degradation rate at 105° is almost twice regarded to the initial degradation rate at 240°. In this case is possible to assure that the resulted amplitude and waveform, even the power is constant in both cases, affect the reactivity in ACE degradation and •OH reactivity. The •OH concentration estimated for 105 and 240° are 77.6 and 56.4 µM respectively. A close ratio of 2.43 and 2.05 µM of •OH per µM of ACE was calculated concomitantly to 52 and 45% of ACE removal by 105 and 240° respectively. Similar main observations were reached for the harmonic case. The initial degradation rate of ACE is 0.42 and 0.32 µM/min for 110 and 45° respectively with a concomitant 65 and 76% of ACE degradation after 120 min of ultrasonic irradiation. In addition, it was observed a near ratio around 2.4 µM of •OH per µM of ACE between both shift angles·H_2O_2 involved in the reaction is slight higher in the case 110° with 45.86 µM against 38.32 µM by adjustment of 45° phase shift. The highest mineralization is observed for 376D case with 8.54% and practically the same for 376R and 3756H cases around 4.5%. In contrast, the BOD_5/BOD_{5o} for 376R and 376H cases is higher than the case 376D. The last finding suggests that different degradation pathways are occurring depending on the dual-frequency signal applied. Even in all cases the initial degradation step is attributable to the hydroxyl radical attack, in the 376D case the higher mineralization suggest that multiple hydroxyl radical attack reach also the first stage of byproducts. Such faster hydroxylation step engages also faster direct mineralization on sulfur and/or nitrogen moieties. However, these byproducts remained in the solution are low biodegradables. In contrast, the 376H and 376R cases are slower in the hydroxylation step and slower mineralization is attributable. However, hidroxylated byproducts increase the biodegradable character of the treated dissolution as suggested by Scheurer, et al., (2012) and Sharma et al., (2012) [9,11].

3.9. UV-US hybrid degradation of ACE

As possible to observe in Figure 7, H_2O_2 concentration remains higher than 25 µM still unreacted after 120 min of US irradiation in practically all D, R and H configurations. The last finding reveals predominant recombination of hydroxyl radicals to form H_2O_2 without further ACE degradation neither relevant mineralization of byproducts. Hydroxylated byproducts as well as H_2O_2 and ACE are highly soluble and hydrophilic and thus ultrasonic degradation would be predominant in the bulk of the solution. Interestingly the higher H_2O_2 production in D case reflects higher reactivity in compression and rarefaction of the bubble with hydroxyl radical attack highly localized around the bubble collapse where •OH reach the bulk previous recombination to H_2O_2. In order to reach higher hydroxyl radical attack by consumption of residual H_2O_2, UV irradiation was considered in simultaneous operation with US irradiation during the first 120 min and additional 120 min without US emission. Fig. 8 depicts the kinetic decay of ACE for the UV-US hybrid system and the H_2O_2 evolution along 240 min of treatment. As possible to observe, additional UV irradiation applied simultaneously to the dual-
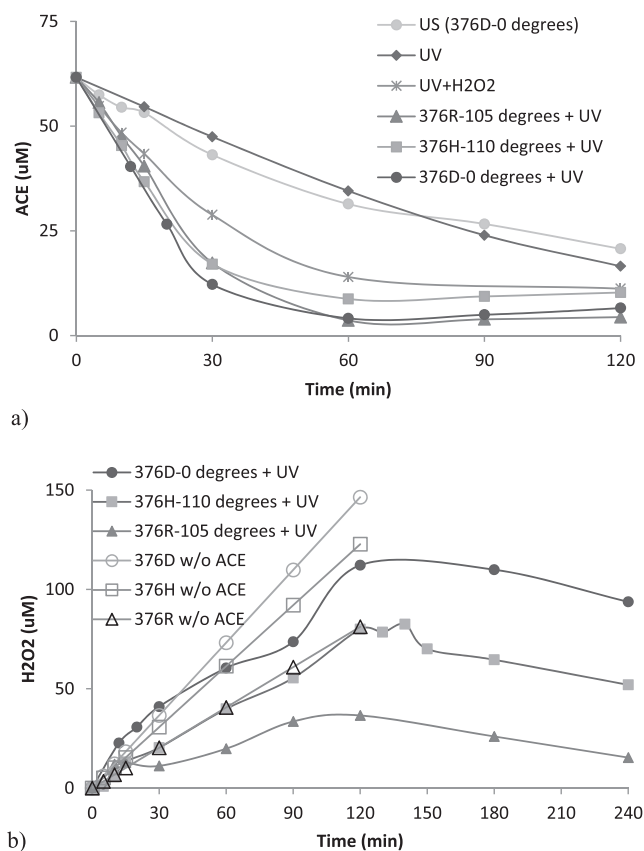

a)

b)

Fig. 8. Simultaneous UV-US hybrid degradation of ACE and H_2O_2 evolution under UV irradiation at extended time. Ar as saturated gas, 1.3 L total volume DW and 6 °C controlled temperature.

frequency irradiation, for particular 376R and 376H cases, improves remarkably the ACE removal rates, mineralization and biodegradability ratio, as also shown in Table 4 and Table 5. The last findings conduct to assume that under R and H configurations the reactivity by bubble collapse are highly distributed in the sonoreactor and the hydroxyl radicals reach easily hydrophilic and hydrophobic byproducts. In contrast, the 376D case slightly improves the ACE removal with marginal TOC and BOD enhancement. It is possible to assure that the most important concentration of hydroxyl radicals and the preferential zone of recombination to H_2O_2 remained closer to the cavitation collapse and that further hydroxyl radical attack is due to H_2O_2 homolysis by UV irradiation. The last effect can be corroborated during the last 120 min of UV irradiation without US emission (Fig. 8b). As possible to observe, the hydroxyl attack continues mineralization of byproducts but in a reduced speed because the degradation by pyrolysis with US regularly distributed in the sonoreactor is not contributing. Fig. 8 also depicts the ACE degradation by UV photolysis, UV + H_2O_2 (oxidant added separately) and 376D irradiation for comparison. Initial degradation rates are 3 and 4 folds higher for UV and UV + H_2O_2 respectively than the analogous by sole D case. Initial degradation rate of ACE by photolysis is 0.4208 µM/min with a remarkable mineralization of 10% and low biodegradability rate. The nitro or sulfur moieties of subproducts are more responsible of such low biodegradability than to the remained H_2O_2 in solution. Such photobyproducts under prolonged UV irradiation are six times more persistent than the parent compound with increased phototoxicity in aquatic ecosystems, as reported in previous work [24]. In contrast, the hybrid system US/UV increases biodegradability and TOC because the average oxidation state increases as well. The important difference in the mineralization suggests that the SO_2 and NC = O functionalities in the anion are the main starting points for degradation by •OH attack by US/UV system and by pyrolysis to the eventual

Table 4

Sonochemical reactivity for photolysis, 376D, UV + H$_2$O$_2$ and hybrid UV-US configurations (376D + UV, 376R + UV and 376H + UV) at optimal modulation and phase shift.

Process	Φ (°)	Initial degradation rate k_{ACE} (µM/min)	ΔH$_2$O$_2$ (µM)	●OH reactivity (µM)	TOC removal 120 min (%)	BOD$_5$/BOD$_{5,ACE10mg/L}$ 120 min
UV	–	0.4208	–	–	10.30	0.5
US (376D)	0	0.5673	70.80	141.6	8.54	0.9
UV + H$_2$O$_2$	–	1.0780	36.90	73.8	4.44	1.5
376D + UV	0	1.6583	34.40	68.8	8.55	1.1
376R + UV	105	1.4821	44.65	89.20	13.86	5.40
376H + UV	110	1.4919	41.57	83.14	14.52	5.01

Table 5

UV reactivity for longer exposition time for residual H$_2$O$_2$ consumption.

	US/UV$_{120\,min}$ + (UV + H$_2$O$_2$ $_{120\,min}$)*		
	H$_2$O$_2$ consumption µM	TOC removal (%) 240 min	BOD$_5$/BOD$_{5,ACE10mg/L}$ 240 min
376D + UV	18.26	9.32	2.5
376R + UV	18.44	15.51	9.56
376H + UV	28.10	16.05	9.55

*Reaction rate 0.2949 ± 0.04 µM H$_2$O$_2$/min for final step without US irradiation.

hydrophobic byproducts generated in 376R and 376H cases [25]. Thus, the three well-defined reaction zones, specially activated in dual-frequencies signals in R and H cases, promote that volatile or hydrophobic subproducts degrade inside the bubble vapor, the ACÉs reactive sites at the bubble interface, and hydrophilic bycompounds at interface or in the bulk aqueous phase assisted by the UV homolysis of H$_2$O$_2$.

3.10. Final remarks

The ultrasound systems by use of single-source double-high frequency signals have a significant potential application in environmental remediation due to their remarkable synergistic effect in hybrid configurations. Phenomenological comprehension of the nature and behavior of the nuclei, growth and collapse of cavitation bubbles generated from a double-frequency signal with much more complex pattern than the sole sine wave requires further research. Moreover, in a practical and realistic point of view, analysis and results with actual effluent containing ACE is strong recommended [17,23] as well as specific analytical determination of subproducts and kinetics. The efficiency of dual-frequencies operation is strong dependent on the physicochemical properties of the targeted organic, byproducts and reaction pathway during degradation (●OH attack based, pyrolytic decomposition or photolysis) [18,22]. Synergy can be reach for specific organics (up to 40% higher than the additive value of the individual frequency operation as shown by Pandit et al., 2006), whereas synergistic effects could not be observed for the degradation of distinct organics which require much higher cavitational intensities and distribution for propagation of different degradation mechanisms. The evolution of byproducts and monitor of the average oxidation state are crucial factors for the US-UV hybrid systems because the final design (sequential or intermittent application of each oxidative step) could improve the biodegradability and reduce toxicity by full depletion of residual H$_2$O$_2$ ultrasonochemically generated. In addition, the scale up requires further research centered in global energy efficiency. Continuous operation and progressive oxidation steps in hybrid configurations are the key requirement for the industrial scale operation.

4. Conclusions

An ultrasound system by use of single-source double-high frequency signal was analyzed for double, resonant and second harmonic cases, 376D, 376R and 376H respectively and applied for ACE degradation.

Additive modulation of waveforms results in more complex pattern than each single sine wave with own selves hydrodynamic character and particularities. Angle phase alignment and percentage of modulation were the most important parameters for improved power distribution (P$_t$) in all cases. However, the highest P$_t$ values along all the angle phase range, from 0 to 360° at 100% modulation, were obtained for 376R and 376H cases. Reactivity measured by H$_2$O$_2$ generation rate in DW resulted in the following performance: 376R < 376D < 376H with 0.58, 1.12 and 1.61 µM/min of H$_2$O$_2$ at 105, 0 and 110° angle shift respectively. However, such behavior does not correspond to a higher degradation of the organic pollutant under similar operating conditions. Initial degradation rate of ACE shown the following sequence: 376R < 376H < 376D with 0.33, 0.42 and 0.56 µM/min respectively agreeing the TOC elimination with 4.74, 4.37 and 8.54%. Contrasting results are observed regard to biodegradability ratio following the next sequence 376D < 376H≈376R with 0.9, 2.30 and 2.33 respectively. Nature of byproducts and their degradation pathway are strong dependent to the dual-frequency signal applied. Composition and physicochemical properties (hydrophobicity, lipophilicity, etc) of ACE and hydroxylated bycompounds promote preferential regions of degradation during the ultrasonic cavitation along the reaction time. Last finding was noteworthy corroborated in the hybrid UV-US system simultaneously and sequentially operated. The hybrid UV-US process stimulates an extra source of hydroxyl radicals by photohomolysis of residual H$_2$O$_2$ sono-generated. The hybrid UV-US process showed synergistic effect in 376D, 376R and 376H cases: higher initial degradation of ACE was observed compared to the observed for the US$_{(D, R\,or\,H)}$ and UV processes alone. Up to 3 folds higher initial degradation of ACE was observed by following the next sequence: 376R≈376H < 376D with 1.49, 1.48 and 1.65 µM/min respectively. Similar synergy behavior up to triple and twice folds higher resulted in TOC elimination (13.86 and 14.52%) and BOD ratio (5.41 and 5.01) remarkably only for the 376R and 376H cases respectively. 376D case showed an insignificant improvement in TOC elimination or biodegradability augment even longer exposition of US or UV source. Improvement of the cavitation phenomena in the 376R and 376H cases is likely related to the intensification of compression and rarefaction events as well as the total acoustic power distribution. Therefore, dual-frequency synergy depends on the specific interactions between the native frequencies, phase shift and percentage of modulation as well as physicochemical character of the byproducts generated, preferential pathways and zone of degradation and the hydrodynamics into the sonoreactor in order to admit the hydroxyl radical recombination or maintain the radical attack together with pyrolysis degradation.

Declaration of Competing Interest

The authors declare that they have no known competing financial interests or personal relationships that could have appeared to influence the work reported in this paper.

Acknowledgements

Appendix A. Supplementary data

Supplementary data to this article can be found online at https://doi.org/10.1016/j.ultsonch.2021.105731.

References

[1] F.T. Lange, M. Scheurer, H.-J. Brauch, Artificial sweeteners -a recently recognized class of emerging environmental contaminants: a review. Anal Bioanal Chem. (2012) Jul;403(9):2503-18. doi: 10.1007/s00216-012-5892-z. Epub 2012 Apr 28. PMID: 22543693.

[2] N. Perkola, P. Sainio (2014) Quantification of four artificial sweeteners in Finnish surface waters with isotope-dilution mass spectrometry. Environ Pollut. 2014 Jan; 184:391-6. doi: 10.1016/j.envpol.2013.09.017. Epub 2013 Oct 5. PMID: 24100049. https://pubmed.ncbi.nlm.nih.gov/24100049/.

[3] Z. Gan, H. Sun, B. Feng, R. Wang, Y. Zhang, Occurrence of seven artificial sweeteners in the aquatic environment and precipitation of Tianjin, China Water Rese. 47 (14) (2013) 4928–4937.

[4] R. Mead, J. Morgan, R. Kieber, A. Kirk, S. Skrabal, J. Willey, Occurrence of the artificial sweetener sucralose in coastal and marine waters of the United States, Mar. Chem. – Mar. Chem. 116 (2009) 13–17, https://doi.org/10.1016/j.marchem.2009.09.005 https://www.sciencedirect.com/science/article/abs/pii/S0304420309001297.

[5] R. Kessler, WATER TREATMENT: Sweeteners Persist in Waterways. Environ Health Perspect. 2009 Oct;117(10):A438. PMCID: PMC2897219. https://www.ncbi.nlm.nih.gov/pmc/articles/PMC2897219/.

[6] M. Scheurer, H.J. Brauch, F.T. Lange, Anal. Bioanal. Chem. 394 (2009) 1585–1594.

[7] L. Son, K.A. Connors, B.W. Brooks, J. Zimmerman, Environ. Sci. Technol. 45 (2011) 1363–1369.

[8] M. Scheurer, F.R. Strock, H.J. Brauch, F.T. Lange, Performance of conventional multi-barrier drinking water treatment plants for the removal of four artificial sweeteners, Water Res. 44 (12) (2010) 3573–3584, https://doi.org/10.1016/j.watres.2010.04.005.

[9] M. Scheurer, M. Godejohann, A. Wick, O. Happel, T. Ternes, H.J. Brauch, W. Ruck, F.T. Lange, Structural elucidation of main ozonation products of the artificial sweeteners cyclamate and acesulfame, Environ. Sci. Pollut. Res. 19 (2012) 1107–1118.

[10] V.K. Sharma, M. Sohn, G.A. Anquandah, Nesnas N Kinetics of the oxidation of sucralose and related carbohydrates by ferrate(VI), Chemosphere 87 (6) (2012) 644–648, https://doi.org/10.1016/j.chemosphere.2012.01.019.

[11] F. Mendez-Arriaga, Doctoral Thesis. Barcelona University 2009.

[12] M. Klavarioti, D. Mantzavinos, D. Kassinos, Removal of residual pharmaceuticals from aqueous systems by advanced oxidation processes, Environ. Int. 35 (2008) 402–417, https://doi.org/10.1016/j.envint.2008.07.009.

[13] Ziye Sang, Yanan Jiang, Yeuk-Ki Tsoi, Kelvin Sze-Yin Leung, Evaluating the environmental impact of artificial sweeteners: a study of their distributions, photodegradation and toxicities, Water Res., 2013.

[14] C.D. Vecitis, H. Park, J. Cheng, B.T. Madre, M.R. Hoffmann, Kinetics and mechanism of the sonolytic conversion of the aqueous perfluorinated sufractants, perfluorooctanoate (PFOA) and perfluorooctane sulfonate (PFOS) into inorganic products. 2008. J. Phys. Chem. A. 112, 4261-4270.

[15] C. Agarkoti, P. Gogate, A. Pandit, Comparison of acoustic and hydrodynamic cavitation based hybrid AOPs for COD reduction of commercial effluent from CETP, J. Environ. Manage. 281 (2020), https://doi.org/10.1016/j.jenvman.2020.111792.

[16] S. Gujar, P. Gogate, P. Kanthale, R. Pandey, S. Thakre, M. Agrawal, Combined oxidation processes based on ultrasound, hydrodynamic cavitation and chemical oxidants for treatment of real industrial wastewater from cellulosic fiber manufacturing sector, Sep. Purif. Technol. 257 (2021), 117888, https://doi.org/10.1016/j.seppur.2020.117888.

[17] A. Camargo-Perea, E. Serna-Galvis, J. Lee, E. Torres-Palma, (2021) Understanding the effects of mineral water matrix on degradation of several pharmaceuticals by ultrasound: Influence of chemical structure and concentration of the pollutants. Ultrasonics Sonochemistry, Volume 73, 2021, 105500, ISSN 1350-4177, doi: 10.1016/j.ultsonch.2021.105500.

[18] Parag R. Gogate, A. Pandit, Cavitation: a technology on the horizon, Curr. Sci. 91 (1) (2006) 35–46.

[19] Parag R. Gogate, A. Pandit, (2004) Sonochemical reactors: scale up aspects, Ultrasonics Sonochemistry, Volume 11, Issues 3–4, May 2004, Pages 105-117.

[20] P.R. Gogate, I.Z. Shirgaonkar, M. Sivakumar, P. Senthilkumar, N.P. Vichare, A.B. Pandit, Cavitation reactors: Efficiency assessment using a model reaction, AIChE J. 47 (11) (2001) 2526–2538.

[21] K. Kawabata, S. Umemura, Use of second-harmonic superimposition to induce Chemical effects of ultrasound, J. Phys. Chem. 100 (1996) 18784–18789.

[22] D. Casadonte, M. Flores, C. Petrier, Enhancing sonochemical activity in aqueous media using power-modulated pulsed ultrasound: an initial study, Ultrason. Sonochem. 12 (2005) 147–152.

[23] J. Cheng, C. Vecitis, H. Park, B. Mader, M. Hoffmann, Sonochemical degradation of perfluorooctane sulfonate (PFOS) and perfluorooctanoate (PFOA) in groundwater: kinetic effects of matrix inorganics, J. Environ. Sci. Technol. 44 (2010) (2010) 445–450.

[24] Z. Sang, S. Jiang, Y. Tsoi, K. Leung, Evaluating the environmental impact of artificial sweeteners: A study of their distributions, photodegradation and toxicities, Water Res. 52 (2013), https://doi.org/10.1016/j.watres.2013.11.002.

[25] Thomas J. Venanzi, A. Carol, A molecular electrostatic-potential study of acesulfame, Anal. Chim. Acta 210 (1988) 213–218.

[26] N.B. Waldo, C.D. Vecitis, Combined effects of phase-shift and power distribution on efficiency of dual-high-frequency sonochemistry, Ultrason Sonochem. 41 (2018) 100–108, https://doi.org/10.1016/j.ultsonch.2017.09.010. Epub 2017 Sep 11 PMID: 29137731.

[27] K. Kawabata, S. Umemura, Effect of Periodic Phase Shift on Acoustic Cavitation Induction with Second-Harmonic Superimposition, Japanese Journal of Applied Physics, (2003), 3246-3250, Vol 42, doi: 10.1143/JJAP.42.3246.

[28] Y. Linzheng, Z. Xijing, H. Yan, S. Tianjiao, Effect of frequency ratio and phase difference on the dynamic behavior of a cavitation bubble induced by dual-frequency ultrasound, Chem. Eng. Processing – Process Intensification 165 (2021), 108448.

[29] K. Kálmán, GPU accelerated numerical investigation of the spherical stability of an acoustic cavitation bubble excited by dual-frequency, Ultrason. Sonochem. 77 (2021), 105684.

[30] P.M. Kanthale, A. Brotchie, M. Ashokkumar, F. Grieser, Experimental and theoretical investigations on sonoluminescence under dual frequency conditions, Ultrason. Sonochem. 15 (2008) 629–635, https://doi.org/10.1016/j.ultsonch.2007.08.006.

[31] A.H. Barati, A. Mokhtari-Dizaji, H. Mozdarani, Z. Bathaie, Z.M. Hassan, Effect of exposure parameters on cavitation induced by low-level dual-frequency ultrasound, Ultrason. Sonochem. 14 (2007) 783–789, https://doi.org/10.1016/j.ultsonch.2006.12.016.